Journal of
Synchrotron Radiation

ISSN 0909-0495

Received 1 May 2010
Accepted 5 August 2010

Development of diamond-based X-ray detection for high-flux beamline diagnostics

Jen Bohon,[a]* Erik Muller[b] and John Smedley[c]

[a]Center for Synchrotron Biosciences, Case Western Reserve University, Upton, NY 11973, USA, [b]Stony Brook University, Stony Brook, NY 11794, USA, and [c]Instrumentation Division, Brookhaven National Laboratory, Upton, NY 11973, USA. E-mail: jbohon@bnl.gov

High-quality single-crystal and polycrystalline chemical-vapor-deposition diamond detectors with platinum contacts have been tested at the white-beam X28C beamline at the National Synchrotron Light Source under high-flux conditions. The voltage dependence of these devices has been measured under both DC and pulsed-bias conditions, establishing the presence or absence of photoconductive gain in each device. Linear response consistent with the theoretically determined ionization energy has been achieved over eleven orders of magnitude when combined with previous low-flux studies. Temporal measurements with single-crystal diamond detectors have resolved the nanosecond-scale pulse structures of both the NSLS and the APS. Prototype single-crystal quadrant detectors have provided the ability to simultaneously resolve the X-ray beam position and obtain a quantitative measurement of the flux.

Keywords: diamond; detector; monitor; position-sensitive; quadrant; white beam; photoconduction; BPM.

1. Introduction

Measurement of monochromatic synchrotron X-ray beam flux is traditionally performed using gas-filled ion chambers and silicon photodiodes. These devices saturate under high-flux conditions, however, necessitating the use of alternative tools for quantitative measurement of broadband and high-flux monochromatic beam flux. The X28C beamline at the National Synchrotron Light Source (NSLS) produces a focused X-ray white beam capable of delivering almost 90 W mm^{-2} to the focal point (Sullivan *et al.*, 2008). Diagnostics for this beam are problematic not only due to saturating levels of flux but also to significant thermal effects that occur at these power densities. Many state-of-the-art synchrotron beamlines face similar challenges. Diamond is a material particularly well suited to addressing these issues as it has a unique combination of mechanical, optical, electronic and thermal properties. The hardness of diamond is unparalleled in a bulk material, making it resistant to mechanical stresses. Diamond is solar-blind, thus insensitive to ambient lighting, and low-Z, allowing considerable X-ray transmission. In addition, diamond has the highest thermal conductivity of any known bulk material and is radiation hard, making it an attractive option for high heat load, high-flux hard X-ray applications (soft X-rays will lose significant flux in the detector, but use of thin material can compensate for this effect to some level). While diamond is currently used for white-beam diagnostics (Shu *et al.*, 1994; Kudo *et al.*, 2006), it has typically been used for its thermal, crystalline or transmission properties. Here we describe diamond-based photoresistors, which also exploit the electronic properties of the material, including the 5.5 eV band gap, the long charge collection distance and the relative equivalence of electron and hole mobilities. Previous development of CVD (chemical vapor deposition) diamond detectors has indicated the promise of these devices (Berdermann *et al.*, 2010; Bergonzo *et al.*, 2000, 2006; Bohon *et al.*, 2010; Kagan, 2005*a*; Keister & Smedley, 2009; Morse *et al.*, 2007, 2008; Schulze-Briese *et al.*, 2001); only recently has diamond material of sufficient quality become readily available to create these diamond 'ion chambers' with near-ideal response (Kagan, 2005*b*). Single- and four-channel single-crystal CVD diamond detectors, as well as a single-channel polycrystalline CVD diamond device, were tested at X28C under a variety of conditions. A linear response was obtained for all powers measured, spanning eleven orders of magnitude (from 0.1 nW to 10 W), including measurements made at both monochromatic and white-beam beamlines (Keister & Smedley, 2009). The diamond was exposed to absorbed X-ray power of the order of a Watt; the incident X-ray flux produced 85 mA of current in the $\sim$0.6 mm^2 area exposed to the beam. In addition, temporal response measurements made at the NSLS and the Advanced Photon source (APS) clearly resolved the storage-ring pulse structures, and suggest that higher biasing and thinner diamond material might provide the capability to measure even shorter timescale signals. Results indicate that this type of diamond detector can be

used as an in-line beam position and flux monitor for both white beam and monochromatic beam with energies higher than ~5 keV, and may provide these metrics for each individual incoming pulse.

2. Experimental

2.1. Single-channel diamond mounts

Two different mounting systems were used for the single-channel diamond detectors (Fig. 1). The 'timing' mount (Fig. 1*a*) was created to hold only the 4 mm × 4 mm single-crystal diamonds, with circular pressure contacts on either side and a rigid coaxial cable which allows timing measurements. The second mount system, the 'claw' mount (Fig. 1*b*), has spring-loaded copper contacts which touch the diamond at a single point on either side of the diamond. This holder allows the use of a range of diamond sizes and can be used in a variety of measurements, including response mapping (performed at X6B); however, the long single-conductor wire leads on this simpler device preclude high-frequency pulse measurement. All devices discussed have sputtered platinum contacts on both sides (ranging from 20–250 nm in thickness); the specifics of this process are described elsewhere (Smedley *et al.*, 2010). Single-crystal diamonds (4 mm × 4 mm, 0.25–0.5 mm thick) were metallized with a 3 mm-diameter pattern, and a polycrystalline diamond (1 cm diameter, 0.21 mm thick) was metallized with a 6 mm-diameter pattern, centered on the diamond such that non-metallized diamond extended beyond the contact to avoid flow of current around the edge of the device. Diamonds (designated 'electronic grade') were obtained from Harris International (now called Element Six)

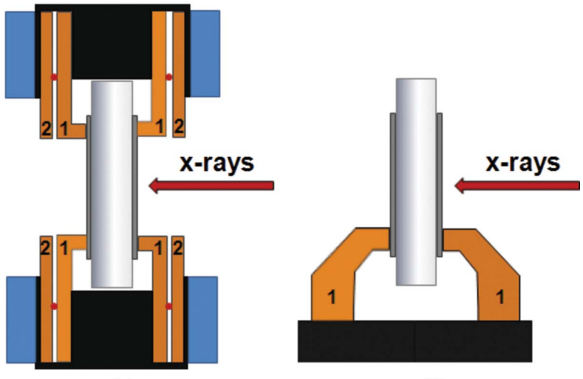

Figure 1
Single-channel diamond mounts. Diamonds are metallized with a layer of Pt on each side. Copper electrodes (orange, labeled 1) contact the diamond. Ceramic insulating material (Macor) is shown in black. (*a*) 'Timing' mount. This holder allows timing measurement, but holds only 4 mm × 4 mm diamonds. Copper photoemission guards (orange, labeled 2) are biased to retard photoemitted electrons from the metal on the diamond surface to ensure that only the signal from the X-ray absorption in the diamond material is measured. Ruby balls (red) insulate the guards from the electrodes. The blue regions represent the stainless steel grounded outer holder. (*b*) 'Claw' mount. This holder can accommodate a range of diamond sizes and can be used for response mapping.

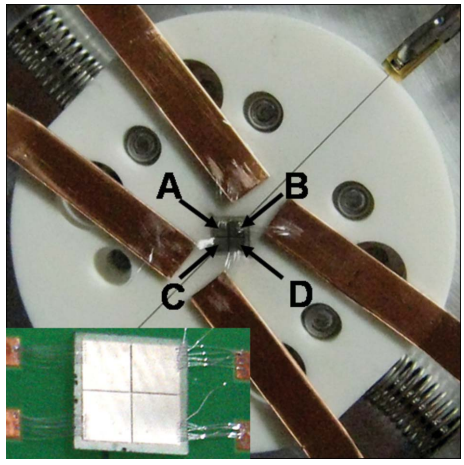

Figure 2
Four-channel detector ('quad') mount. The diamond is held in the mount under compression from the edges (note the springs). Each pad of the detector (labeled *A*–*D* and indicated with arrows) is wire-bonded to copper electrodes. Inset: close-up view of a similar device mounted to a PCB board. The diamonds shown are 4 mm × 4 mm, the metallization ends 0.25 mm from the edge of the diamond and the spacing between metallized regions is 50 µm.

and were processed at the Element Six facility in Ascot, UK. Diamond surfaces were polished to a 4 nm r.m.s. roughness.

2.2. Four-channel diamond mount

The four channels of the quad detector (Fig. 2) were created by sputtering platinum onto a masked single-crystal diamond. The mask is laser-cut silicon, shaped into a cross pattern with 50 µm arms. Ten wire bonds using 25 µm Al wire (with 1% Si) were made between the platinum surface and the copper electrode for each quadrant. The detector was held in spring-loaded ceramic (Macor) jaws which clamped the edges of the diamond. A single pressure contact was made with the solid back side electrode for biasing.

2.3. Beamline configurations

The focused white-beam X28C beamline at the NSLS is capable of producing a range of power densities and spot sizes up to a maximum of ~90 W mm^{-2} in a focused 0.5 mm-diameter spot with a broad energy range (5–15 keV) (Sullivan *et al.*, 2008). This allows access to a range of broadband flux values through focusing of the mirror and the use of aluminium filters of various thicknesses (0.08–4.5 mm); the effects on the spectrum can be calculated using known X-ray properties of the elements (Henke *et al.*, 1993; http://henke.lbl.gov/optical_constants/). Two beam sizes were used for these experiments, ~1.1 mm vertical × 0.55 mm horizontal (~0.6 mm^2), and ~2 × 7 mm (14 mm^2) with a 1.6 mm-diameter aperture (~2 mm^2). A traditional ion chamber (windowless, filled with dry N_2 gas) is used for calibration of strongly attenuated beam; a copper calorimeter (3.4431 g) is used for calibration of beams which saturate the ion chamber. A schematic of the experimental set-up is shown in Fig. 3. Initial measurements were performed in air, causing signifi-

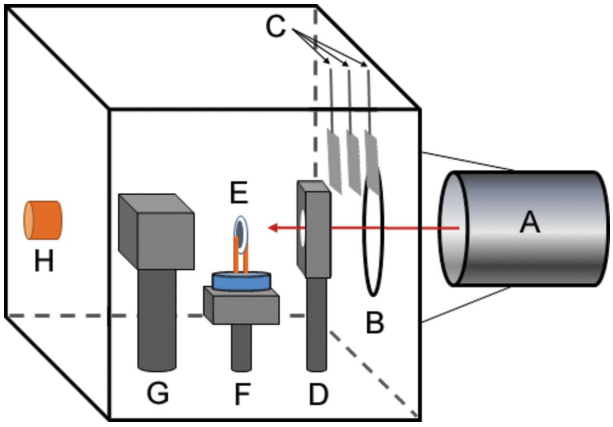

Figure 3
X28C experimental set-up. X-rays exit the beampipe (A) through the terminal 0.076 mm aluminium window, enter an N_2-filled enclosure through an aperture (B) sealed to the beampipe to maintain the N_2 atmosphere and may pass through attenuators (C) and a 1.6 mm-diameter aperture (D) before striking the diamond (E). The diamond is mounted on a stand (F) which can translate in a two-dimensional plane perpendicular to the beam. The beam path through nitrogen from the end of the vacuum beampipe to the diamond is ∼145 mm. The beam then passes through a 95 mm-long ion chamber (G) (∼40 mm from the diamond) and strikes a copper calorimeter (H) (∼150 mm from the diamond).

cant damage to the metal contacts owing to high ozone concentrations created by the X-ray beam; thus a dry-nitrogen-purged enclosure was built for subsequent experiments. Initially, the beampipe was kept in a vacuum; however, focusing of the mirror in later experiments caused sufficient heating of the X28C beamline terminal 0.076 mm aluminium exit window to melt a hole and break the vacuum; later experiments were performed with a helium purge on the beampipe, leaving the pinhole in the window. Bias was applied to the X-ray incident surface of the diamond and current was measured from the opposite side using Keithley electrometers (models 617, 6514 and 6517A) for currents up to 10 mA and Fluke multimeters for higher currents (four in the case of the quadrant detector). Both DC and pulsed voltages were applied for reasons which will be discussed. Pulsed biasing was accomplished using a high-voltage amplifier (FLC electronics A800DI) combined with a function generator (Keithley 3390). The pulsed bias consists of a square wave with an 'on time' defined by a duty cycle and a frequency, typically 1 kHz.

X-ray beam mapping was performed at NSLS beamline X6B using a photon energy of 19 keV and a beam spot of 100 µm × 100 µm (a 20 µm × 20 µm spot was used for fine scans). The diamonds were mounted under ambient conditions in the claw holder (Fig. 1*b*). A Si diode positioned behind the diamond was used both for flux calibration and to align the diamond (93% of the photons go through the diamond to the diode). The X-ray response of the diamond was measured with electrometers as described above.

Timing measurements were made at APS beamline 11-ID-D using monochromatic X-rays at 12 keV, at NSLS beamline U3C using soft X-ray white beam (0.2–1 keV) and at NSLS beamline X28C using hard X-ray white beam (5–15 keV). The timing mount (Fig. 1*a*) was used for all timing experiments. Measurements at 11-ID-D were made both in air and Ar. After 12 h of continuous exposure to the undulator beam in air, the contacts exhibited visible damage (and an associated degradation in signal level), presumably owing to ozone. Subsequent analysis *via* scanning electron microscopy indicated that the damage was likely due to a change in the contact rather than the diamond material (data not shown). Measurements performed within an Ar atmosphere avoided this damage. The flux was calibrated with ion chambers both before and after the diamond. An Agilent Infinium DSO80804B oscilloscope (8 GHz bandwidth) coupled with a Herotec AF0018333A amplifier (20 GHz bandwidth) was used to observe the timing structure from the detector. Timing data were collected in a vacuum at U3C using a Tektronix TDS5104 oscilloscope and a ×10 B&H Electronics AC5020H20 amplifier (both 3 GHz bandwidth). A Tektronix TDS694c oscilloscope (no amplifier, 3 GHz bandwidth) was used for measurements at NSLS X28C.

3. Detector calibration

Single-crystal and polycrystalline devices were studied under high-flux conditions; single-crystal devices have also been calibrated at lower fluxes at monochromatic beamlines (Keister & Smedley, 2009). The combined results of these measurements indicate that the linearity of this calibration spans eleven orders of magnitude, six of which are shown in Figs. 4 and 5(*a*), performed at X28C. Response calibration plots for additional single-crystal detectors are shown in Fig. S2.[1] The low-flux data collected previously at monochromatic beamlines yielded a mean ionization energy (w) (also referred to as the electron–hole pair creation energy) of 13.3 eV (Keister & Smedley, 2009). The results of the present experiments indicate that this value also well predicts the response over a further six orders of magnitude for both single-crystal and polycrystalline diamond. This value for the ionization energy is consistent with both theoretically calculated and previously measured values (Dimitrov *et al.*, 2010; Ziaja *et al.*, 2005), indicating a charge collection distance greater than the thickness of the device for these measurements. Construction of multiple channels on these devices did not impact the observed charge collection.

Calibration of each device was performed *via* comparison with an ion chamber at lower fluxes and a copper calorimeter at high flux. A standard deviation of 10% was used for ion chamber measurements based on an observed maximal deviation of 10% in the ion chamber value over the 400 V diamond bias sequences. Calorimetric determinations of power absorbed in the diamond were performed by subtraction of data with and without the diamond in the beam path (taking into account the platinum layers). Error in the individual calorimetric measurements was determined from the

[1] Supplementary data for this paper are available from the IUCr electronic archives (Reference: GF5027). Services for accessing these data are described at the back of the journal.

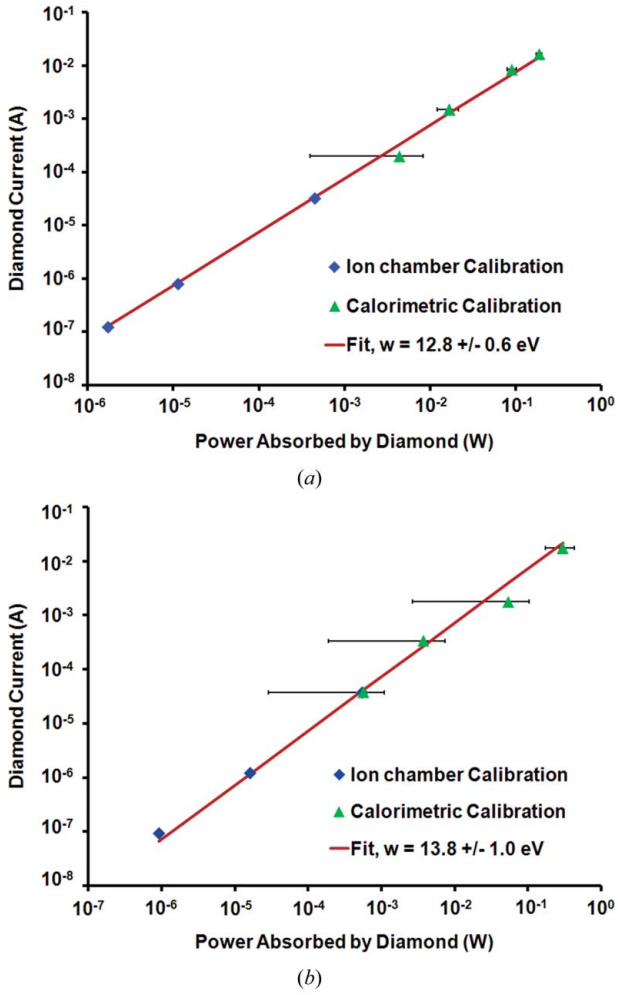

Figure 4
Response calibration of single-channel detectors. (*a*) Single-crystal diamond (0.5 mm thickness, 300 V DC bias), measured in the timing mount. (*b*) Polycrystalline diamond (0.21 mm thickness, 200 V DC bias), measured in the claw mount.

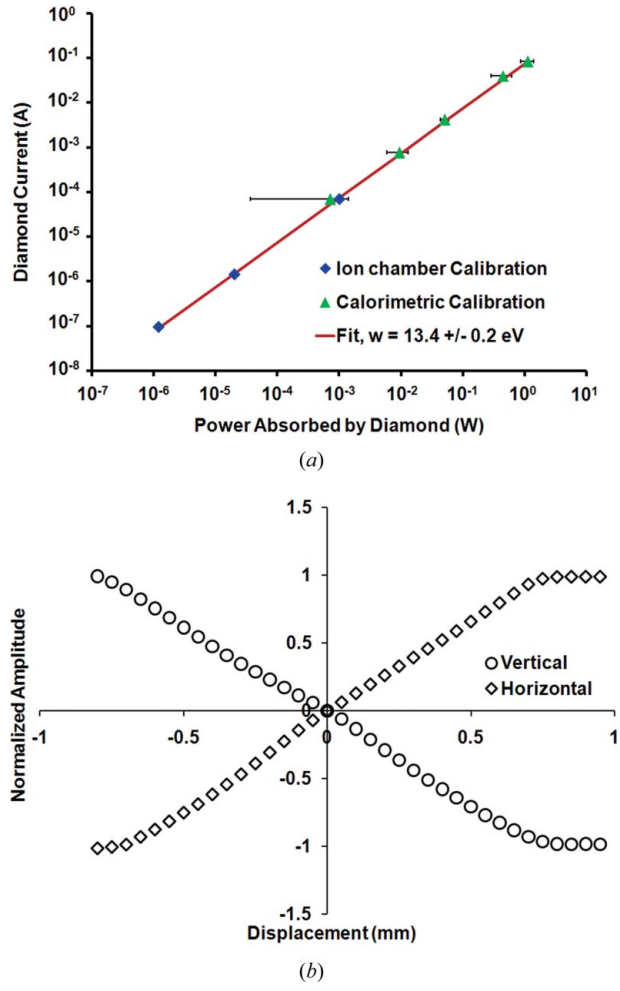

Figure 5
Quadrant detector measurement. (*a*) Response calibration and (*b*) positional calibration of a single-crystal quad detector.

standard deviation in the absorbed power determined from each heating step (measured once per second) in the exposure. The number of heating steps ranged from a maximum of 180 s for highly attenuated beam, resulting in a total temperature jump of 0.8 K, to a minimum of 50 s for strongly focused unattenuated beam, resulting in a temperature jump of 185 K (this corresponds to a maximum temperature of >473 K, which threatened to destabilize the Lucite insulator contacting the calorimeter). The error values determined for measurements in the presence and absence of diamond were added in quadrature to obtain the standard deviations used in the calibration calculation. The slope of the line was fit *via* χ^2 minimization to determine the ionization energy calibration. All error values reported (Figs. 4 and 5) represent single standard deviations.

The positional response of the four-channel detector (Fig. 5*b*) was tested by translating the device linearly from center in the horizontal and vertical dimensions across the beam. The vertical response was calculated as $[(A + B) - (C + D)]/(A + B + C + D)$ and the horizontal response as $[(A + C) - (B + D)]/(A + B + C + D)$ as defined in Fig. 2. The slope of the line was fit *via* χ^2 minimization; the resulting calibration was used with the measured values to calculate the expected position, and the standard deviation of these from the actual motor positions was defined as the resolution (6.5 µm vertical, 3.5 µm horizontal). It should be stressed that the stated resolution is a convolution of four factors: the detector resolution, the motor control system resolution, the beam size and the beam drift owing to fluctuations inherent in the accelerator electron orbit. The deviation from linearity observed in Fig. 5(*b*) is likely due to fluctuations in incident beam position during the experiment. Although no specific data were taken to quantify the beam drift, a casual observation of the signal drift when the detector was stationary indicated that this effect was not insubstantial and is therefore probably the dominant effect determining the resolution in this measurement. No attempt was made to determine the actual resolution of the device within the scope of the reported experiments because 6.5 µm was well within the resolution requirements of the beamline.

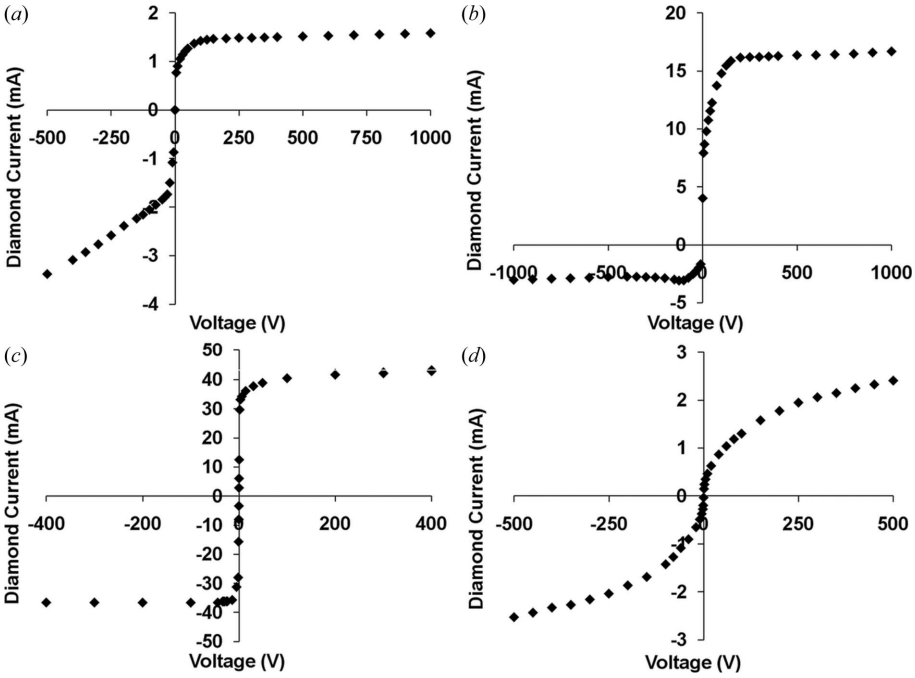

Figure 6
Voltage dependence of (*a*) PC single-crystal DC bias, (*b*) PC single-crystal DC positive bias, pulsed negative bias, (*c*) non-PC single-crystal DC bias and (*d*) polycrystalline diamond DC bias.

4. Voltage dependence

Fig. 6 shows the dependence of the device response on voltage. Leakage currents were measured to be negligible (<1 pA) for single-crystal devices and 190 pA for the polycrystalline device at a field of 0.3 MV m^{-1}. In general, once full carrier collection has been achieved, the signal increase ends and the response becomes independent of voltage. For the single-crystal diamond device shown in Fig. 6(*a*) this occurs for positive biasing, but negative bias creates a linearly increasing signal with voltage after the initial phase, the hallmark of photoconductive (PC) gain. At the inflection point the bias becomes high enough that the carriers injected owing to trapped charge can move across the entire thickness of the diamond before they can be trapped or can neutralize the trapped charge (Knoll, 2000). As this injection can occur many times before the trapped charge is neutralized, we observe an associated gain in current. The addition of a pulsed-bias cleaning cycle allows detrapping of the material and is able to 'turn off' the photoconductive gain; in this case (Fig. 6*b*), a 10% duty cycle was used for the negative polarity, while the positive bias was applied DC. Fig. 6(*c*) depicts the response of a non-PC single-crystal diamond, which exhibits back-to-back diode-like behavior even under the highest flux conditions measured. X-ray topography and response mapping has indicated that this diamond is free of electrically active point defects in the active area (Muller *et al.*, 2010). This is not the case for the photoconductive diamond, as will be discussed later. Fig. 6(*d*) shows the voltage dependence of a polycrystalline diamond. The characteristics of this curve are different in two ways from the single-crystal case: the slope of the rise leading to saturation is lower, and the signal does not plateau but continues to gradually rise for all voltages measured. The expected response value is obtained at the transition between these phases, suggesting that PC gain may play a role in the subsequent response increase with voltage.

5. Timing

Timing measurements were performed on single-crystal diamonds at NSLS beamlines X28C (5–15 keV) and U3C (0.2–1 keV), and also at APS beamline 11-ID-D (12 keV). Fig. 7 shows timing measurements of the NSLS bunch structure provided during the experiment. Of the 30 ~1 ns buckets available, 25 were filled, leaving five empty for ion cleaning. Fig. 8 compares timing measurements of a non-PC diamond at

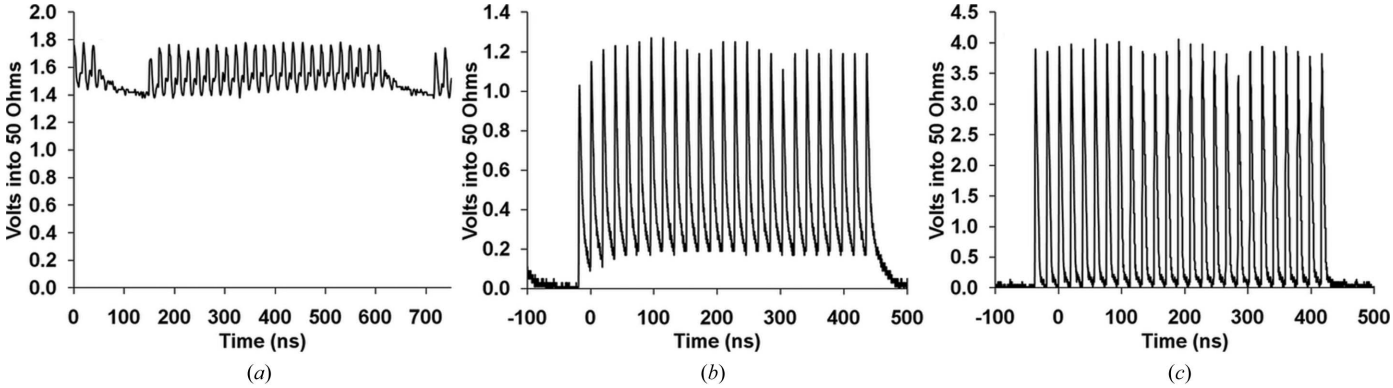

Figure 7
Timing measurements. (*a*) Photoconductive (PC) diamond, 100 V DC bias (0.3 MV m^{-1} field), (*b*) non-PC diamond, 150 V bias (0.3 MV m^{-1}), 50% duty cycle and (*c*) non-PC diamond, 1000 V DC bias (2 MV m^{-1} field).

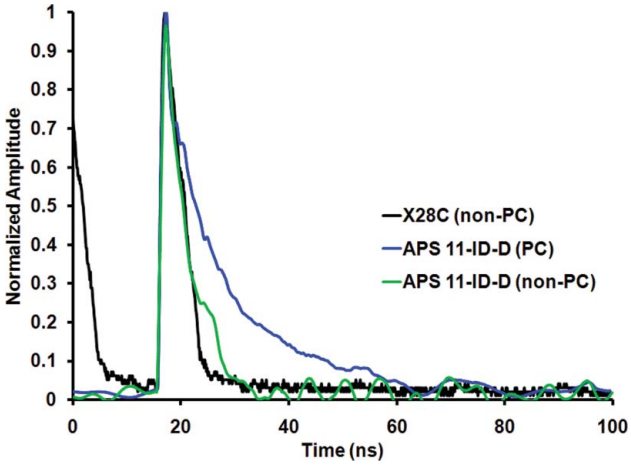

Figure 8
Normalized timing measurements performed at the APS. Non-PC (green) and PC (blue) diamond exposed to monochromatic (12 keV) X-rays at 11-ID-D (0.7 MV m^{-1} field). The non-PC timing measurement (2 MV m^{-1} field) for the high-flux X-ray white beam at X28C (black) is included for comparison.

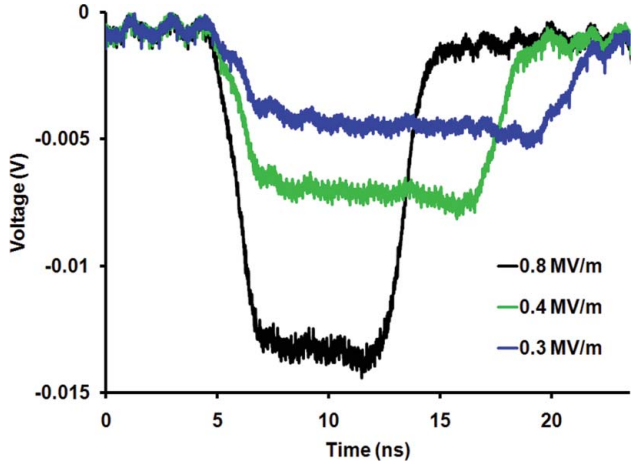

Figure 9
Pulse width as a function of field in the diamond. This measurement uses broadband soft X-rays (0.2–1 keV). Increased field decreases the carrier transit time. The voltage is measured into 50 Ω using a ×10 amplifier.

X28C under high-flux white-beam conditions with those for both PC and non-PC diamonds at 11-ID-D at the APS in a 12 keV monochromatic X-ray beam.

In all timing measurements the observed pulse width is broadened owing to the transit time of the carriers; the thickness of the diamond and the strength of the applied field determine the timing capabilities. While the rise is limited by the incident pulse width (∼1 ns for the NSLS, 100 ps for the APS) and the electronics bandwidth, the decay is related to carrier transit. In the PC devices [Figs. 7(*a*) and 8 (blue line)] the decay is much longer, and is determined by the lifetime of the injected carrier; in this particular case we believe that the trapped carriers are electrons and that holes are injected (Smedley *et al.*, 2010). In Fig. 7(*a*) the PC gain has reached a steady state of trapping and detrapping, thus the high steady baseline. In Fig. 8 (blue line) the time between pulses is considerably longer (∼150 ns compared with ∼20 ns for the NSLS), allowing the photoconductive response to end before the next pulse arrives. The non-PC device under low biasing conditions (Fig. 7*b*) also illustrates the effect of carrier mobility on the timing resolution; here, the bias is not strong enough to drive the carriers across the diamond before the next incident pulse except during the ion cleaning cycle, creating an elevated baseline during the 25 bunch series. Under high voltage (Fig. 7*c*) the bias is able to move the carriers across in much less than the ∼18.9 ns of the bunch period, bringing the signal back to zero between pulses. It is important to note that the current values calculated from these traces are also consistent with average current measurements on the electrometers for all devices characterized.

The fall time seen for the non-PC devices in Figs. 7 and 8 can be attributed to the creation of carriers throughout the diamond. In a traditional time-of-flight measurement, performed using α particles, only one carrier crosses the full thickness of the diamond, resulting in a square-wave signal (Pernegger *et al.*, 2005). This can also be illustrated using soft X-rays (0.2–1 keV), where the carriers are all generated very near the incident surface of the diamond. As all of the carriers are moving a similar distance, this results in a square-wave-like pattern (Fig. 9). As the voltage applied to the diamond is increased, the resulting field increases the velocity of the carriers (Fig. S1), decreasing the pulse width. However, in the case of the broadband (5–15 keV) and monochromatic high-energy (12 keV) X-ray beams (Figs. 7 and 8), the radiation easily penetrates the bulk of the diamond, creating carriers at a continuum of distances from the collection electrode. This results in an associated continuum of times required for carrier collection, up to the time required to travel the full device thickness. In all cases, those carriers created furthest from the electrode will determine the full signal width, thus higher pulse rate timing capabilities will be obtained with thinner diamonds.

6. Lifetime

For high-flux applications which require temporal resolution, considerable voltages are needed; high current draw through the diamond is the major cause of heating of the device. If timing measurements are not required, these types of detectors can be operated at low voltage (50 V), which will significantly decrease the heat load and simplify mounting and cooling requirements. The contact material used must be robust in the environment in which it will be used; early copper contacts disintegrated when in the beam path, likely due to ozone produced in the air nearby; all subsequent high-flux experiments have been performed in a nitrogen environment with platinum contacts to avoid this possibility. It is important to note that, for high-flux measurements thus far, blocking contacts cannot be maintained. Once exposed to high-flux X-ray irradiation, the temperatures that the detectors reach cause the loss of oxygen from the diamond surface (Keister *et al.*, 2010; Mori *et al.*, 1991; Smedley *et al.*, 2010) and a subsequent change in the contact nature.

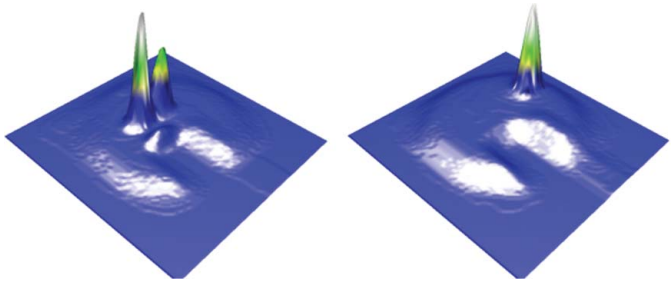

Figure 10
Response maps of PC single-crystal diamond. The rectangular pattern inset into the diamond response is the area occluded by the claw mount (data taken at X6B at 19 keV, 100 V bias in each polarity, 80% duty cycle). The x and y axes are the physical dimensions of the diamond (4 mm × 4 mm). For negative bias (left), the base diode level (dark blue) is -38 ± -1 pA and the maximum response (white) is -970 pA. For positive bias (right), the base diode level (dark blue) is 39 ± 1 pA and the maximum response (white) is 450 pA.

Response mapping of the annealed contacts of the PC single-crystal diamond clearly illustrates the isolated nature of the PC spots (Fig. 10) (Guerrero *et al.*, 2004). The negative-bias response map indicates that there are two PC spots within the target area for the incident beam, while the only PC spot on the positive response map falls outside of that area and would therefore not be observable. These PC spots have been shown to correlate with point defects in the diamond using X-ray topography (Muller *et al.*, 2010); diamonds which do not contain these defects do not exhibit PC gain (Fig. 6*c*), indicating that improving the quality of the diamond within the detection region will result in diode-like behavior in devices constructed from this material.

7. Conclusions

We have demonstrated that CVD diamond detectors can perform well over a wide range of flux values and can also be used for temporal profiling of the beam. Both the quality and thickness of the diamond material used determine the biasing requirements to achieve the desired measurement capabilities of a given device. For simple flux measurements using single-crystal devices >250 µm in thickness with no timing requirements, the operating bias can be as low as 50 V. As the parameter of importance is the effective electric field in the diamond, thinner material can further reduce the necessary applied bias. The theoretical mean ionization energy can be used for flux calibration (given a known spectrum, in a manner similar to a traditional ion chamber) of both single-crystal and polycrystalline devices, including the four-channel quadrant single-crystal detectors constructed for simultaneous flux and beam position measurements. Measurement of the beam position at X28C under high-flux conditions was well within the modest requirements of the beamline; ongoing studies include characterization of the resolution of the quadrant detectors under conditions which will better determine the limitations of the devices themselves.

The authors wish to thank John Walsh for design and fabrication of sample mounts, Xiangyun Chang for assistance with metallization and Bin Dong for technical assistance. The team is further indebted to Veljko Radeka, Pavel Rehak and Jeffrey W. Keister for discussion and guidance over the course of this work, to Klaus Attenkofer and the team at APS 11-ID-D for their assistance with the timing experiments, and to Mark Chance for providing access to the resources at the Case Center for Synchrotron Biosciences. The authors wish to acknowledge the support of the US Department of Energy (DOE) under grant DE-FG02-08ER41547 and the National Institute for Biomedical Imaging and Bioengineering under P30-EB-09998. This manuscript has been authored by Brookhaven Science Associates, LLC, under Contract No. DE-AC02-98CH10886 with the US DOE. Use of the National Synchrotron Light Source beamlines X28C, U3C and X6B was also supported by the DOE under the aforementioned contract. Use of the Advanced Photon Source was supported by the DOE, Office of Science, Office of Basic Energy Sciences, under Contract No. DE-AC02-06CH11357.

References

Berdermann, E., Pomorski, M., de Boer, W., Ciobanu, M., Dunst, S., Grah, C., Kis, M., Koenig, W., Lange, W., Lohmann, W., Lovrincic, R., Moritz, P., Morse, J., Mueller, S., Pucci, A., Schreck, M., Rahman, S. & Trager, M. (2010). *Diamond Relat. Mater.* **19**, 358–367.

Bergonzo, P., Brambilla, A., Tromson, D., Mer, C., Hordequin, C., Guizard, B., Foulon, F., Sole, V. A. & Gauthier, C. (2000). *Diamond Relat. Mater.* **9**, 960–964.

Bergonzo, P., Tromson, D. & Mer, C. (2006). *J. Synchrotron Rad.* **13**, 151–158.

Bohon, J., Smedley, J., Muller, E. & Keister, J. W. (2010). *Diamond Electronics and Bioelectronics – Fundamentals to Applications III, Materials Research Society Symposium Proceedings Series*, Vol. 1203, p. J19-03. Warrendale: Materials Research Society.

Dimitrov, D. A., Busby, R., Cary, J. R., Ben-Zvi, I., Smedley, J., Chang, X., Rao, T., Keister, J. W., Muller, E. & Burrill, A. (2010). *Diamond Electronics and Bioelectronics – Fundamentals to Applications III, Materials Research Society Symposium Proceedings Series*, Vol. 1203, p. J17-43. Warrendale: Materials Research Society.

Guerrero, M. J., Tromson, D., Barrett, R., Tucoulou Tachoueres, R. & Bergonzo, P. (2004). *Phys. Status Solidi A*, **201**, 2529–2535.

Henke, B. L., Gullikson, E. M. & Davis, J. C. (1993). *Atom. Data Nucl. Data Tables*, **54**, 181–342.

Kagan, H. (2005*a*). *Nucl Instrum. Methods Phys. Res. A*, **541**, 221–227.

Kagan, H. (2005*b*). *Nucl Instrum. Methods Phys. Res. A*, **546**, 222–227.

Keister, J. W. & Smedley, J. (2009). *Nucl Instrum. Methods Phys. Res. A*, **606**, 774–779.

Keister, J. W., Smedley, J., Dimitrov, D. & Busby, R. (2010). *IEEE Trans. Nucl. Sci.* Submitted.

Knoll, G. F. (2000). *Radiation Detection and Measurement*, 3rd ed., p. 491. NewYork: Wiley.

Kudo, T., Takahashi, S., Nariyama, N., Hirono, T., Tachibana, T. & Kitamura, H. (2006). *Rev. Sci. Instrum.* **77**, 123105.

Mori, Y., Kawarada, H. & Hiraki, A. (1991). *Appl. Phys. Lett.* **58**, 940–941.

Morse, J., Salome, M., Berdermann, E., Pomorski, M., Cunningham, W. & Grant, J. (2007). *Diamond Relat. Mater.* **16**, 1049–1052.

Morse, J., Salome, M., Berdermann, E., Pomorski, M., Grant, J. O'Shea, V. & Ilinski, P. (2008). *Diamond Electronics – Fundamentals to Applications II, Materials Research Society Symposium Proceedings Series*, Vol. 1039, p. P06-02. Warrendale, PA: Materials Research Society.

Muller, E., Smedley, J., Raghothamachar, B., Gaowei, M., Keister, J. W., Ben-Zvi, I., Dudley, M. & Qiong, W. (2010). *Diamond Electronics and Bioelectronics – Fundamentals to Applications III, Materials Research Society Symposium Proceedings Series*, Vol. 1203, p. J17-19. Warrendale: Materials Research Society.

Pernegger, H., Roe, S., Weilhammer, P., Frais-Kolbl, H., Griesmayer, E., Kagan, H., Schnetzer, S, Stone, R., Trischuk, W., Twitchen, D. & Whitehead, A. (2005). *J. Appl. Phys.* **97**, 073704.

Schulze-Briese, C., Ketterer, B., Pradervand, C., Bronnimann, Ch., David, C., Horisberger, R., Puig-Molina, A. & Graafsma, H. (2001). *Nucl. Instrum. Methods Phys. Res. A*, **467–468**, 230–234.

Shu, D., Collins, J. T., Barraza, J. & Kuzay, T. M. (1994). *Nucl. Instrum. Methods Phys. Res. A*, **347**, 577–580.

Smedley, J., Keister, J. W., Muller, E., Jordan-Sweet, J., Bohon, J., Distel, J. & Dong, B. (2010). *Diamond Electronics and Bioelectronics – Fundamentals to Applications III, Materials Research Society Symposium Proceedings Series*, Vol. 1203, p. J17-21. Warrendale: Materials Research Society.

Sullivan, M., Rekhi, S., Bohon, J., Gupta, S., Abel, D., Toomey, J. & Chance, M. R. (2008). *Rev. Sci. Instrum.* **79**, 025101.

Ziaja, B., London, R. A. & Hajdu, J. (2005). *J. Appl. Phys.* **97**, 064905.